Helical spin structure in iron chains with hybridized boundaries

Cite as: Appl. Phys. Lett. 117, 213105 (2020); https://doi.org/10.1063/5.0022926 Submitted: 31 July 2020 . Accepted: 19 October 2020 . Published Online: 25 November 2020

🧓 Nicolas M. Vargas, 🗓 Felipe Torres, 🗓 Alexander A. Baker, et al.







ARTICLES YOU MAY BE INTERESTED IN

Chiral symmetry and scale invariance breaking in spin chains AIP Advances 10, 025215 (2020); https://doi.org/10.1063/1.5130190

Fast Fourier transform and multi-Gaussian fitting of XRR data to determine the thickness of ALD grown thin films within the initial growth regime

Applied Physics Letters 117, 213106 (2020); https://doi.org/10.1063/5.0024991

Acoustoelectric drag current in vanadium oxide films

Journal of Applied Physics 128, 155104 (2020); https://doi.org/10.1063/5.0015215





Helical spin structure in iron chains with hybridized boundaries

Cite as: Appl. Phys. Lett. **117**, 213105 (2020); doi: 10.1063/5.0022926 Submitted: 31 July 2020 · Accepted: 19 October 2020 · Published Online: 25 November 2020







Nicolas M. Vargas, ^{1,a)} D Felipe Torres, ^{2,3} D Alexander A. Baker, Donathan R. I. Lee, Donathan R. I.

AFFILIATIONS

- Department of Physics and Center for Advanced Nanoscience, University of California, San Diego, La Jolla, California 92093, USA
- ²Department of Physics, Universidad de Chile, Santiago 7800024, Chile
- Center for the Development of Nanoscience and Nanotechnology, CEDENNA, Santiago 9170124, Chile
- ⁴Materials Science Division, Lawrence Livermore National Laboratory, Livermore, California 94550, USA
- ⁵Department of Physics and Astronomy, University of Texas at San Antonio, San Antonio, Texas 78249, USA
- ⁶General Atomics, PO Box 85608, San Diego, California 92186, USA

ABSTRACT

We have compared the magnetic properties of well-controlled ultra-short (\leq 50 nm) atomic iron (Fe) chains embedded in Fe-phthalocyanine films with those in Fe-hydrogen (H₂) phthalocyanine superlattices. Surprisingly, we found that the coercivity of the atomic chains with free boundary conditions is independent of the chain length, whereas the one subject to hybridization of the chain ends exhibits an unexpected length dependence. These findings suggest that ferromagnetism in the free-boundary condition system is caused by an intrinsic indirect exchange. On the other hand, controlled boundary conditions produce a helical spin structure due to an extrinsic indirect exchange, which arises from the interaction between iron atoms at the ends of the chain and the hydrogen in the H₂ phthalocyanine spacer. As a consequence, during magnetic reversal, ultra-short iron chains subject to boundary clamping develop a helical spin structure, leading to increased coercivity. These findings suggest unique insights and ideas for the design of atomic-scale ultra-dense magnetic storage nanodevices.

Published under license by AIP Publishing. https://doi.org/10.1063/5.0022926

As the size of a magnetic structure is reduced, the effect of thermal fluctuations becomes more disruptive, preventing magnetic ordering. Nevertheless, extra sources of magnetic anisotropy that quench fluctuations may stabilize low-dimensional magnetic order. In one-dimensional (1D) magnetic systems, long-range ferromagnetic order can be achieved by the interaction between the magnetic atoms and their supporting frames, such as substrates or inert (non-magnetic) crystal lattices, in which the system is embedded. These interactions produce magnetic anisotropy barriers that, in combination with slow magnetic relaxation, stabilize magnetic order. This discovery and the physical realization of 1D systems with magnetic interactions have become essential to address pressing problems such as quantum criticality, and the emergence of new (topological) magnetic phases the ones predicted by Haldane. In a specific prevention of the support of the s

We have investigated the magnetism of one-dimensional atomic chain between 7 and 150 atoms using well-controlled metallo-phthalocyanine films. For this, we compared 1D iron phthalocyanine (FePc) chains with either free boundary conditions or FePc/metal-free

phthalocyanine (H_2Pc) superlattices (SLs) with hybridized end atoms. Both display magnetic order below 30 nm. Although structurally identical, free boundary condition 1D FePc displays length independent coercivity, whereas for FePc/ H_2Pc superlattices, the coercivity increases as a function of length.

The magnetism of these atomic chain magnets is due to indirect exchange interactions between the delocalized π electrons of aromatic rings and localized unpaired d-shell electron spin of Fe atoms. $^{22-26}$ As a result, super-exchange interaction through Fe–N–Fe ions leads to ferromagnetism in chains with free ends. An anisotropic Dzyaloshinskii–Moriya interaction (DMI) arises from the inclusion of spin–orbit interaction in chains with hybridized ends. This leads to the formation of very unusual helical spin structures as well as interface symmetry breaking in chains with hybridized ends. This explains the experimental differences in the coercivity observed in the two systems.

Metallo-phthalocyanines are planar molecules with a metal atom located at the center of the molecule surrounded by an organic support. Analysis Many atoms (including Fe) and also two H (H₂Pc) can be incorporated as central atoms, as shown in Fig. 1(a). These

a) Author to whom correspondence should be addressed: nvargasayala@physics.ucsd.edu

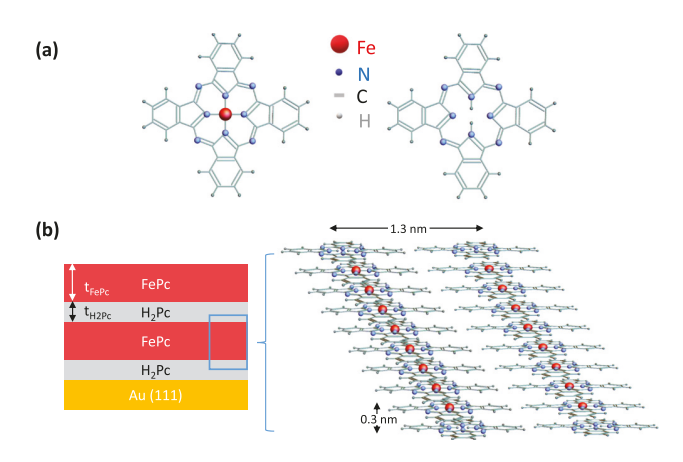


FIG. 1. Schematic representation of FePc chain SLs. Magnetic moments of the Fe atoms (red circles) lie in a plane parallel to the Au-substrate. The Fe end atoms, at the FePc/ H_2 Pc interface, are subject to a weak local anisotropy induced by the Fe/ H_2 electronic hybridization. The thicknesses of H_2 Pc and FePc layers are represented by t_{H2} Pc and t_{FePc} , respectively.

molecules stack face-to-face, parallel to the substrate, 27,32,33 when grown by organic molecular beam epitaxy (OMBE) on Au-coated sapphire. A schematic illustration of the 1D Fe chain based on FePc/H₂Pc SLs is presented in Fig. 1(b). The thickness of the FePc (t_{FePc}) controls the Fe chain length, and the intercalated H_2Pc layers ($t_{H2}Pc = 5 \text{ nm}$) provide controlled boundary conditions, as seen below. The lateral separation between the chains is 1.3 nm, and it is determined by the organization of the molecules on the substrate as shown in Fig. 1(b). The physical structure of the chains is determined quantitatively using high resolution $\theta - 2\theta$ x-ray diffraction (XRD). The molecule axes organize at $\sim 60^{\circ}$ with respect to the sample surface. Experimentally, much progress has been made in the fabrication of 1D systems. 36-40 However, the control of the size, orientation, and composition of the chains is limited, which prevents the experimental determination of the extent and persistence of short- and long-range magnetic interactions and how these interactions are affected by magnetic or electronic boundary conditions induced at the end of the chains. Here, we used a state-of-the-art fabrication method of macroscopic arrays of 1D iron chains that utilizes iron phthalocyanine (FePc) thin films and FePc/metal-free phthalocyanine (H₂Pc) superlattices (SLs). This method allows the precise control of the chain length and orientation and bonding environments for the iron (Fe) atoms at the end of the chains.

FePc/ H_2 Pc SLs and single FePc films were simultaneously grown on Au-coated (0001) sapphire substrates and (0001) sapphire substrates as reference samples. Figure 2 shows the $\theta-2\theta$ x-ray diffraction (XRD) peak corresponding to the (400) peak of reference samples for different FePc thicknesses. The XRD spectrum of the SLs is characterized by the appearance of clear cut satellite peaks, which confirms the layered structure of the SLs, preserving the stacking arrangement. Quantitative information was obtained using the SUPREX refinement technique. 41,42 This refinement yields the average number and standard deviation of H_2 Pc (FePc) monolayers within each H_2 Pc (FePc) layer and the average d-spacing (monolayer-to-monolayer distance) perpendicular to the substrate surface for both, H_2 Pc and FePc, molecular layers. The 1.5–2.8 nm variance in the

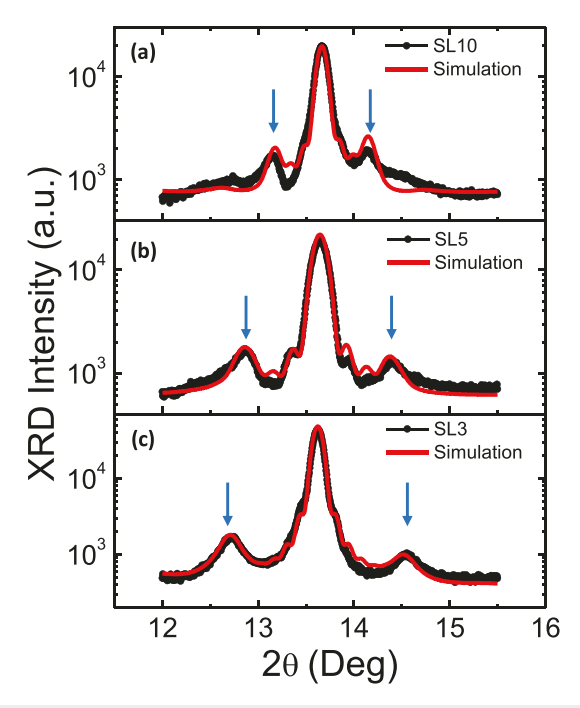


FIG. 2. X-ray diffraction and SUPREX simulation of SLs grown on (0001) sapphire. The XRD (400) peaks corresponding to (top) SL10: (FePc 10 nm/H₂Pc 5 nm)_{x2}, (middle) SL5: (FePc 5 nm/H₂Pc 5 nm)_{x4}, and (bottom) SL3: (FePc 3 nm/H₂Pc 5 nm)_{x8} are displayed. Blue arrows indicate the superlattice satellite peak position.

thickness of the layers corresponds to a roughness of 1–2 monolayers when the molecules are oriented perpendicular to the sapphire substrate. Since the SLs and single FePc films on sapphire and Au-coated substrates were simultaneously deposited, the growth conditions are similar. This roughness provides an error bar in the determination of the chain lengths.

The electronic hybridization and local bonding environment of the FePc films and SLs were determined from X-ray Absorption Spectroscopy (XAS). The Fe L-edge XAS results are presented in Fig. 3, which show the angular dependence of the absorption at the Fe L_{2,3} edges, measured in total electron-yield mode at 300 K. Data have been corrected for fluctuations in incident light intensity using I₀ measured on a gold grid immediately upstream of the measurement chamber. A linear background has been subtracted and the pre-edge to post-edge step scaled to 1 to allow comparisons between samples. The XAS of 20 nm FePc layers in a film and a SL [Fig. 3, showing grazing (a) and normal (b) incidence] show a similar spectral shape but reveal a modification in line shape, particularly at normal incidence. The SL displays a fully resolved peak at 705 eV (related to a_{1g} and e_g orbitals, the latter that are hybridized with the π -ligands of the phthalocyanine), and sharply decreased spectral weight at 706.7 eV (attributed to in-plane b_{1g} orbitals, associated with antibonding states).

Angle-dependent XAS measurements confirm that the molecules stack with their planes parallel to the substrate. The bonding environment found in the C, N XAS is not modified, suggesting that the electronic character of the organic framework around the 1D magnetic chains is not significantly altered by its incorporation into the SL

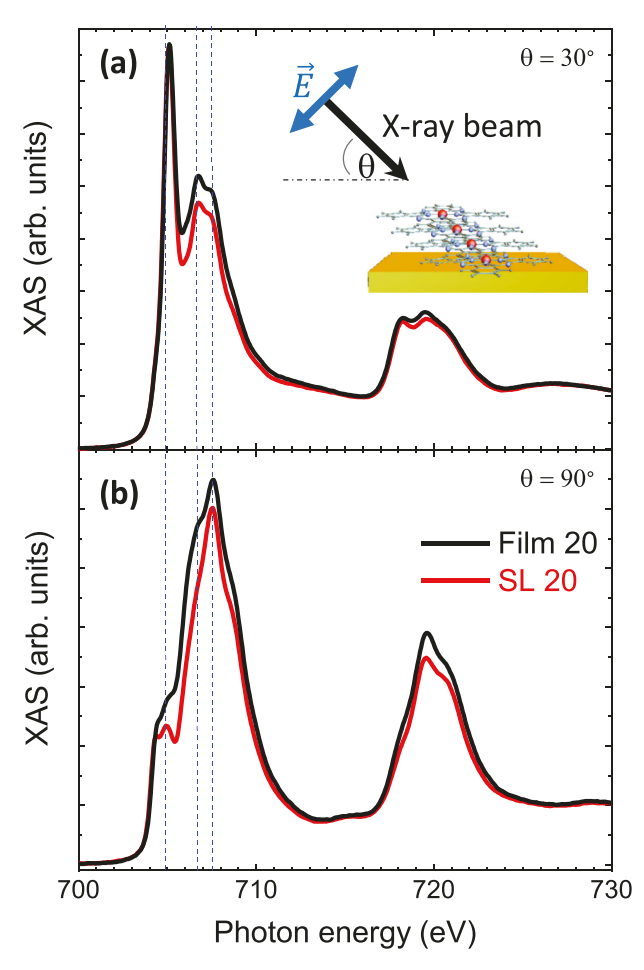


FIG. 3. Comparison between XAS measurements of films (black lines) and SLs (red lines) for (a) $\theta=30^\circ$ and (b) $\theta=90^\circ$. The small peak at 705 eV observed at $\theta=90^\circ$ in the SL is an indication of the hybridization with the π -ligands of FePc with H₂Pc. The significant loss of the spectral weight between $\theta=30^\circ$ and $\theta=90^\circ$ at 706.7 eV is associated with in-plane b_{1g} orbitals. A schematic representation of the measurement setup is given as the inset in (a).

structure. The use of SLs provides two advantages over simple FePc films: it increases the magnetic volume of the sample by increasing the number of repetitions (e.g., the number of FePc layers) and it provides an extra source of anisotropy for the Fe atoms at the interfaces with $\rm H_2Pc$ due to Fe–H hybridization. In this way, the magnetic signal of ultra-short (as little as seven atoms long) Fe chains can be measured by a conventional vibrating sample magnetometer (VSM), and the electronic states of the Fe atoms at the end of the chains can be modified in a controlled manner.

Magnetic hysteresis loops at low temperatures and up to a field of 10 kOe were performed in a VSM of a Quantum Design DynaCool system [see Fig. 4(a)]. During field scans, the temperature stability was better than 1%, and the field sweep rate was 20 Oe/s. In all measurements, the field was applied parallel to the substrate surface. The dependence of the saturation magnetic moment at 1.8 K as a function of the FePc layer thickness for both SLs and films grown on Au is

shown in Fig. 4(b). As expected, the total magnetic moment of films and SLs (divided by the number of periods) scales linearly with the total amount of FePc deposited in each sample.

The coercivities were extracted from low temperature magnetic (VSM) hysteresis loops for films and SLs grown on Au-coated substrates. Figure 4 shows the coercivity dependence as a function of chain length. Surprisingly, the coercivity of the films is independent of chain length [Fig. 4(c)], whereas SLs show a definite coercivity increase as a function of length, well beyond any possible experimental error [Fig. 4(d)]. This linear dependence holds even for the shortest chains $(t_{\text{FePc}} = 3 \text{ nm} \text{ and } 5 \text{ nm})$, which could only be measured in SLs. Remarkably, there is a significant difference between the coercivity evolution with the FePc thickness between films and the SLs for the same total chain length. Experimentally, the only difference between these two is the boundary condition at the end of the chain. The element-selective XAS measurements discussed above show that the Fe 3d orbitals of the FePc, in proximity to the H₂Pc layers, are strongly modified. This gives rise to an additional magnetic anisotropy at the end of the chains, which can be incorporated into a model to explain the experimental observations quantitatively.

Although experimental evidence indicates that the spin-orbit coupling takes place in these spin chains, 33,44-46 the role of Dzyaloshinskii-Moriya interaction (DMI) is generally neglected, possibly because its contribution to large chains is unimportant. As the number of spins in the chain decreases, the effect of the DMI on the energy barrier is enhanced. In SLs, the DMI is due to the spin-orbit interaction; it splits the 3d Fe orbitals with a planar D_{4h} symmetry, 4 while the inversion symmetry breaking at the FePc/H₂Pc interface, which accounts for the spin canting at the ends of the chains, is induced by electronic hybridization. As a result, chiral states induced at the ends of the chains dominate the reversal mode, which naturally displays a size-dependent behavior due to the wavelength of the emergent helical spin structure. 48-50 At the atomic scale, thermal fluctuations overcome the direct exchange, and dipolar interactions do not affect intrachain behavior. Therefore, the inclusion of an effective DMI, which accounts for spin canting, is crucial to describe the sizedependent magnetic behavior of the FePc superlattices and provides physical parameters in agreement with experimental results. As a consequence, the spin-orbit interaction stabilizes a helical spin structure, which leads to the unusual change observed in the coercivity. To provide a physical mechanism for the above results, we have developed a semi-classical analytical model. The energy of a 1D chain, oriented along the z-axis, is

$$E = -\sum_{i} \left[J\vec{s}_{i} \cdot \vec{s}_{i+1} + \vec{D}_{i,i+1} \cdot (\vec{s}_{i} \times \vec{s}_{i+1}) + K(\vec{s}_{i} \cdot \hat{e}_{i}) \right], \quad (1)$$

where J is the exchange coupling between neighboring Fe atoms and $\bar{D}_{i,i+1} = (-1)^i D\hat{z}$ is the antisymmetric Dzyaloshinskii–Moriya tensor. $\hat{e}_i \neq 0$ for the chain end atom and zero otherwise. The DMI, induced by localized electrons, is oriented perpendicular to the substrate. To obtain the coercivity and the hysteresis loop, we minimize the energy, Eq. (1). Locally, a parallel spin configuration is energetically preferred by the ferromagnetic exchange interaction, while a canted spin configuration is favored by the DMI. The competition between these two interactions gives rise to two oppositely handed helical spin structures, where the handedness depends on the sign of DMI. The interaction between two Fe ions, nearest to the $H_2Pc/FePc$ interface, through the

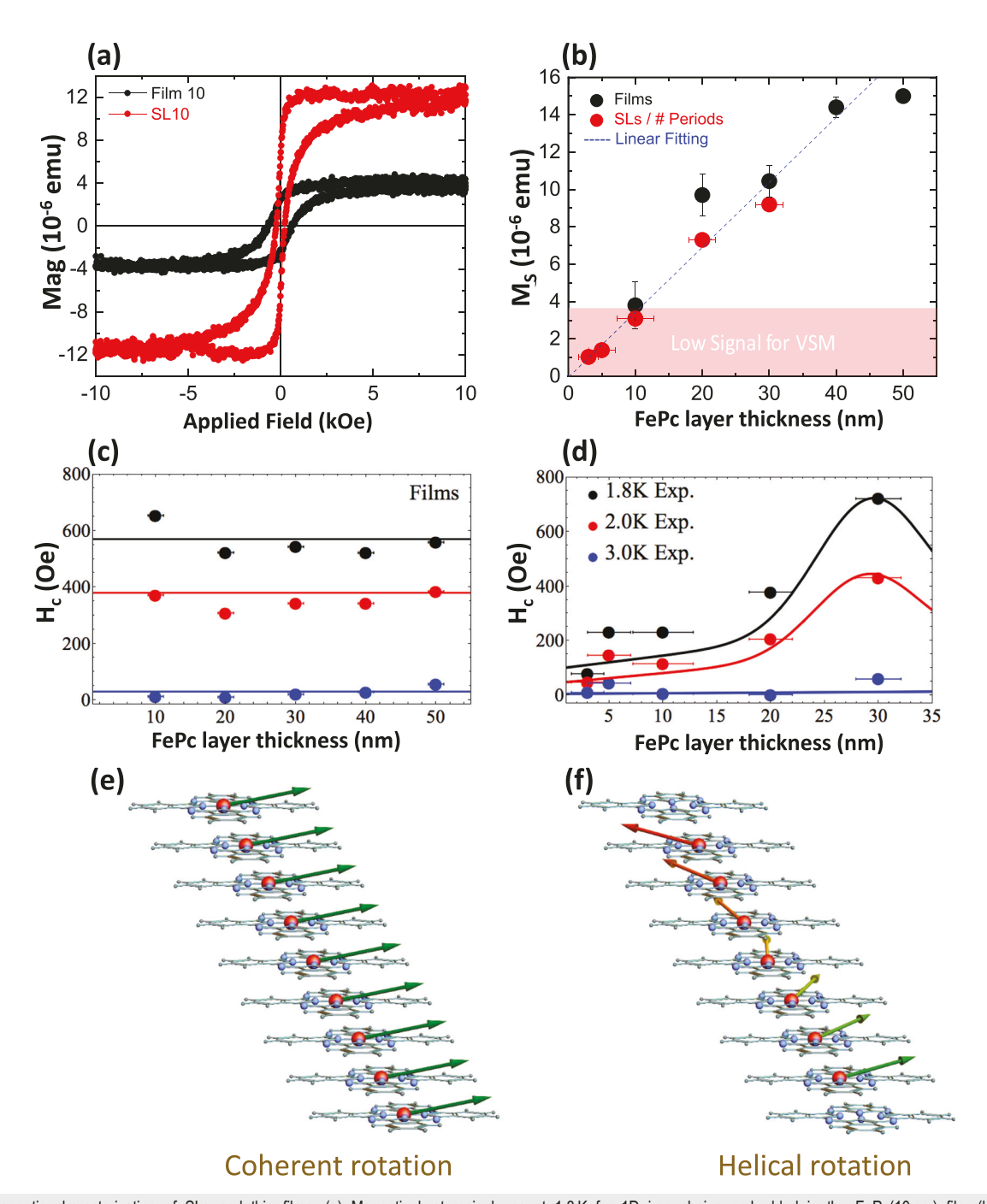


FIG. 4. Magnetic characterization of SLs and thin films. (a) Magnetic hysteresis loops at 1.8 K for 1D iron chains embedded in the FePc(10 nm) film (black) and SL10 = FePc(10 nm)/H₂Pc(5 nm)]_{x4} superlattice (red). (b) Lineal dependence of the saturation magnetic moment vs total FePc thickness for films (black circles) and SLs (red circles). The magnetic moment of each SL is divided by its number of periods. The blue line is a linear fit to the data. The low VSM signal region indicates that FePc films below 10 nm do not have enough magnetic signal to be measured by the VSM. SLs with ultra-thin FePc layers of 1.5 and 3 nm thicknesses can be measured because the number of repetitions (8 and 4, respectively) increases the magnetic volume of the samples. Coercivity dependence on the chain length for (c) FePc thin films and (d) FePc/ SLs. As the FePc thickness increases, the coercivity remains constant in thin films (c), whereas it increases linearly in the SLs (d). The comparison between experimental results (full circles) and the theoretical prediction (continuous lines) is in excellent agreement. In SLs, the thickness error bars were estimated by the SUPREX refinement software. 41,42 For films, the error bars are smaller than the filled dots. (e) Coherent reversal mode in the single free Fe spin chain. (f) Magnetization reversal mode induced by the chiral symmetry breaking in a Fe spin chain with boundary conditions.

 $\rm H_2$ breaks the symmetry of the chain. Due to the misalignment at $\rm H_2Pc/FePc$, the interaction at the interfaces gives rise to an effective anisotropy at the chain ends. When DMI has opposite directions at the ends of the chain, which means that the weak anisotropies are also aligned in opposite directions, the boundary condition produces left-and right-handed reversal modes. This chiral symmetry breaking produces two states with opposite chirality. The competition between them generates a local anisotropy on the central magnetic moments of the chain, which depends on the size of the helicoidal arrangement. This additional spatial periodicity causes the magnetic reversal mode to depend on the chain length.

This model yields a coherent rotation of the Fe chain magnetic moments subject to free boundary conditions (K=0), as in films, and a magnetization reversal process governed by an asymmetric chiral rotation for the weakly end-pinned spins in the SLs $(K\neq 0)$. The same length Fe chains in films and SLs display different magnetic responses due to differing boundary conditions. For films, the coherent rotation of the magnetic moments of the Fe chains is independent of the chain length and results in the absence of coercivity changes, see Fig. 4(e). However, in the SLs, the small hybridization at the chain ends breaks this symmetry, causing a helical chiral spin state that produces a length dependent coercivity, see Fig. 4(f).

At large enough magnetic fields, the magnetic moments of the chain are fully saturated along the applied magnetic field direction. During magnetization reversal, at intermediate magnetic fields, magnetic moments located at both ends of the chain experience an additional torque due to the boundary conditions, tilting away from the rest of the magnetic moments of the chain in opposite directions.

The formation of the helical state with magnetization rotation in opposite directions arises from the competition between the magnetic interactions and the symmetry breaking. This in turn produces two helical spin waves of opposite chirality that propagate from the two chain ends. At the center of the chain, the balance between these two states induces an effective anisotropy as the applied field is increased sufficiently to suddenly reverse and align the magnetic moments in the central region. This becomes apparent in the energy increase required to complete the magnetic reversal, which in turn increases the coercivity. Therefore, due to the propagation of helical states from the chain ends, the coercivity is strongly dependent on the chain length.

There is excellent agreement between the experimental results and the theoretical model, as shown in Fig. 4. Notice that there are only three adjustable parameters in the model: the exchange interaction $J/k_B=4.5\,\rm K$, the Dzyaloshinskii–Moriya coupling strength $D=10^{-2}\,\rm J$, and the magnetic anisotropy $K=10^{-4}\,\rm J$. Moreover, it is quite remarkable that the DMI, due to the Fe–H coupling at the end of the Fe chains, provides sufficient interaction energy that creates additional anisotropy to stabilize the 1D magnetization. This may be the first case in which an additional anisotropy in a one-dimensional system is due to a boundary condition acting on the end atoms and does not extend over the whole length of the magnetic chain.

In conclusion, we have discovered an unexpected coercivity increase as a function of length in 1D FM chains with hybridized boundary conditions. This effect was obtained by comparing OMBE synthesized arrays of well-controlled, ultra-short Fe chains, using FePc films and FePc/H₂Pc superlattices. Our method provides a technique to amplify the magnetic signal of ultra-short 1D FM chains, composed

of as few as seven atoms. High-resolution quantitative XRD shows control at the atomic level over the whole length 1D Fe chains.

In SLs, element-selective XAS measurements show that the Fe orbitals of the FePc boundaries experience local bonding changes when in proximity to the H₂Pc layers. These electronic changes at the end of the chains produce noticeable effects on their magnetic properties. The coercive field of the chains grown as SLs (i.e., subject to hybridization) increases with length, whereas the coercive field of chains grown as films (i.e., not subject to hybridization) remains constant.

An analytical model, which yields asymmetric helical order due to a small anisotropy at the chains ends, explains the results quantitatively. This is an example of an exotic type of one-dimensional helical magnetic order produced by DMI, which could encourage further development of the technological research based on the helical-magnetic ordering of a few atoms.

We are grateful to T. Gredig and D. Altbir for useful discussions. This collaborative UCSD-UTSA research was supported by NSF under Grant Nos. DMR 1805585 and DMR 1804414. F. Torres and M. Kiwi acknowledge financial support from Grant Nos. FA9550-161-0122, FA9550-18-1-0438, Fondecyt 1160639, and CEDENNA through the Financiamiento Basal para Centros Científicos y Tecnológicos de Excelencia-FB0807. The Lawrence Livermore National Laboratory is operated by Lawrence Livermore National Security, LLC, for the U.S. Department of Energy, National Nuclear Security Administration under Contract No. DE-AC5207NA27344. This work was partially supported by the LLNL-LDRD program under Project No. 19-LW-028. Part of this research used resources of the Advanced Light Source, which is a DOE Office of Science User Facility under Contract No. DE-AC02-05CH11231.

DATA AVAILABILITY

The data that support the findings of this study are available from the corresponding author upon reasonable request.

REFERENCES

- ¹N. D. Mermin and H. Wagner, "Absence of ferromagnetism or antiferromagnetism in one- or 2-dimensional isotropic Heisenberg models," Phys. Rev. Lett. 17(22), 1133 (1966).
- ²J. Eisenmenger and I. K. Schuller, "Overcoming thermal fluctuations," Nat. Mater. 2, 437 (2003).
- ³V. Skumryev, S. Stoyanov, Y. Zhang, G. Hadjipanayis, D. Givord, and J. Nogués, "Beating the superparamagnetic limit with exchange bias," Nature 423, 850 (2003).
- ⁴F. Torres, D. Altbir, and M. Kiwi, "Dzyaloshinskii-Moriya interaction and magnetic ordering in 1D and 2D at nonzero T," Europhys. Lett. **106**(4), 47004 (2014)
- ⁵S. Sachdev, "Quantum criticality: Competing ground states in low dimensions," Science 288(5465), 475–480 (2000).
- ⁶B. C. Watson, V. N. Kotov, M. W. Meisel, D. W. Hall, G. E. Granroth, W. T. Montfrooij, S. E. Nagler, D. A. Jensen, R. Backov, M. A. Petruska, G. E. Fanucci, and D. R. Talham, "Magnetic spin ladder (C₅H₁₂N)₂ CuBr₄: High-field magnetization and scaling near quantum criticality," Phys. Rev. Lett. 86(22), 5168–5171 (2001).
- ⁷B. Lake, D. A. Tennant, C. D. Frost, and S. E. Nagler, "Quantum criticality and universal scaling of a quantum antiferromagnet," Nat. Mater. 4, 329 (2005).
- ⁸R. Coldea, D. A. Tennant, E. M. Wheeler, E. Wawrzynska, D. Prabhakaran, M. Telling, K. Habicht, P. Smeibidl, and K. Kiefer, "Quantum criticality in an

- Ising chain: Experimental evidence for emergent E_8 symmetry," Science 327(5962), 177–180 (2010).
- ⁹M. Girardeau, "Relationship between systems of impenetrable bosons and fermions in one dimension," J. Math. Phys. 1(6), 516–523 (1960).
- ¹⁰C. N. Yang, "Some exact results for the many-body problem in one dimension with repulsive delta-function interaction," Phys. Rev. Lett. 19(23), 1312–1315 (1967).
- ¹¹H. L. Haselgrove, M. A. Nielsen, and T. J. Osborne, "Entanglement, correlations, and the energy gap in many-body quantum systems," Phys. Rev. A 69(3), 032303 (2004).
- ¹²T. J. Osborne and N. Linden, "Propagation of quantum information through a spin system," Phys. Rev. A 69(5), 052315 (2004).
- ¹³Z. Zanolli, G. Onida, and J. C. Charlier, "Quantum spin transport in carbon chains," ACS Nano 4(9), 5174–5180 (2010).
- ¹⁴C. Ramanathan, P. Cappellaro, L. Viola, and D. G. Cory, "Experimental characterization of coherent magnetization transport in a one-dimensional spin system," New J. Phys. 13(10), 103015 (2011).
- ¹⁵E. Coronado and M. Yamashita, "Molecular spintronics: The role of coordination chemistry," <u>Dalton Trans.</u> 45(42), 16553–16555 (2016).
- ¹⁶C. Pang, A. Srivastava, M. M. Lockart, T. Mewes, M. K. Bowman, N. Bao, L. Shen, and A. Gupta, "Magnetic properties of semiconducting spinel CdCr₂S₄ nanostructured films grown by low-pressure metal-organic chemical vapor deposition," ACS Appl. Electron. Mater. 1(8), 1424–1432 (2019).
- 17 J. Camarero and E. Coronado, "Molecular vs. inorganic spintronics: The role of molecular materials and single molecules," J. Mater. Chem. 19(12), 1678–1684 (2009).
- ¹⁸B. Balasubramanian, P. Manchanda, R. Pahari, Z. Chen, W. Zhang, S. R. Valloppilly, X. Li, A. Sarella, L. Yue, A. Ullah, P. Dev, D. A. Muller, R. Skomski, G. C. Hadjipanayis, and D. J. Sellmyer, "Chiral magnetism and high-temperature skyrmions in B20-ordered Co-Si," Phys. Rev. Lett. 124(5), 057201 (2020).
- ¹⁹C. O. Avci, E. Rosenberg, L. Caretta, F. Büttner, M. Mann, C. Marcus, D. Bono, C. A. Ross, and G. S. D. Beach, "Interface-driven chiral magnetism and current-driven domain walls in insulating magnetic garnets," Nat. Nanotechnol. 14(6), 561–566 (2019).
- ²⁰F. D. M. Haldane, "Nonlinear field theory of large-spin Heisenberg antiferromagnets: Semiclassically quantized solitons of the one-dimensional easy-axis Néel state," Phys. Rev. Lett. 50(15), 1153–1156 (1983).
- ²¹F. D. M. Haldane, "Continuum dynamics of the 1-D Heisenberg antiferromagnet: Identification with the O(3) nonlinear sigma model," Phys. Lett. A 93(9), 464–468 (1983).
- ²²J. Bartolomé, C. Monton, and I. K. Schuller, "Magnetism of metal phthalocyanines," in *Molecular Magnets: Physics and Applications*, edited by J. Bartolomé, F. Luis, and J. F. Fernández (Springer Berlin Heidelberg, Berlin, Heidelberg, 2014), pp. 221–245.
- ²³W. Wu, A. Kerridge, A. H. Harker, and A. J. Fisher, "Structure-dependent exchange in the organic magnets Cu(II)Pc and Mn(II)Pc," Phys. Rev. B 77(18), 184403 (2008).
- ²⁴M. Grobosch, C. Schmidt, R. Kraus, and M. Knupfer, "Electronic properties of transition metal phthalocyanines: The impact of the central metal atom (d5–d10)," Org. Electron. 11(9), 1483–1488 (2010).
- ²⁵N. Marom and L. Kronik, "Density functional theory of transition metal phthalocyanines, I: Electronic structure of NiPc and CoPc—self-interaction effects," Appl. Phys. A 95(1), 159–163 (2009).
- T. Kroll, R. Kraus, R. Schönfelder, V. Y. Aristov, O. V. Molodtsova, P. Hoffmann, and M. Knupfer, "Transition metal phthalocyanines: Insight into the electronic structure from soft x-ray spectroscopy," J. Chem. Phys. 137(5), 054306 (2012).
- ²⁷F. Bartolomé, O. Bunău, L. M. García, C. R. Natoli, M. Piantek, J. I. Pascual, I. K. Schuller, T. Gredig, F. Wilhelm, A. Rogalev, and J. Bartolomé, "Molecular tilting and columnar stacking of Fe phthalocyanine thin films on Au(111)," J. Appl. Phys. 117(17), 17A735 (2015).
- ²⁶J. Bartolomé, F. Bartolomé, L. M. García, G. Filoti, T. Gredig, C. N. Colesniuc, I. K. Schuller, and J. C. Cezar, "Highly unquenched orbital moment in textured Fe-phthalocyanine thin films," Phys. Rev. B 81(19), 195405 (2010).

- ²⁹P. D. Ekstrand, D. J. Javier, and T. Gredig, "Tunable finite-sized chains to control magnetic relaxation," Phys. Rev. B 95(1), 014406 (2017).
- ³⁰T. Gredig, M. Werber, J. L. Guerra, E. A. Silverstein, M. P. Byrne, and B. G. Cacha, "Coercivity control of variable-length iron chains in phthalocyanine thin films," J. Supercond. Nov. Magn. 25(7), 2199–2203 (2012).
- ³¹R. Otero, J. M. Gallego, A. L. V. de Parga, N. Martín, and R. Miranda, "Molecular self-assembly at solid surfaces," Adv. Mater. 23(44), 5148–5176 (2011).
- ³²C. Monton, I. Valmianski, and I. K. Schuller, "The role of micro-shorts and electrode-film interface in the electrical transport of ultra-thin metallophthalocyanine capacitive devices," Appl. Phys. Lett. 101(13), 133304 (2012).
- ³³F. Freimuth, S. Blügel, and Y. Mokrousov, "Berry phase theory of Dzyaloshinskii-Moriya interaction and spin-orbit torques," J. Phys. 26(10), 104202 (2014).
- 34C. W. Miller, A. Sharoni, G. Liu, C. N. Colesniuc, B. Fruhberger, and I. K. Schuller, "Quantitative structural analysis of organic thin films: An x-ray diffraction study," Phys. Rev. B 72(10), 104113 (2005).
- 35T. Gredig, C. N. Colesniuc, S. A. Crooker, and I. K. Schuller, "Substrate-controlled ferromagnetism in iron phthalocyanine films due to one-dimensional iron chains," Phys. Rev. B 86(1), 014409 (2012).
- ³⁶P. Gambardella, A. Dallmeyer, K. Maiti, M. C. Malagoli, W. Eberhardt, K. Kern, and C. Carbone, "Ferromagnetism in one-dimensional monatomic metal chains," Nature 416, 301 (2002).
- ³⁷P. Gambardella, S. Rusponi, M. Veronese, S. S. Dhesi, C. Grazioli, A. Dallmeyer, I. Cabria, R. Zeller, P. H. Dederichs, K. Kern, C. Carbone, and H. Brune, "Giant magnetic anisotropy of single cobalt atoms and nanoparticles," Science 300(5622), 1130–1133 (2003).
- ³⁸S. Fölsch, P. Hyldgaard, R. Koch, and K. H. Ploog, "Quantum confinement in monatomic Cu chains on Cu(111)," Phys. Rev. Lett. **92**(5), 056803 (2004).
- ³⁹C. F. Hirjibehedin, C. P. Lutz, and A. J. Heinrich, "Spin coupling in engineered atomic structures," Science 312(5776), 1021–1024 (2006).
- ⁴⁰P. Ferstl, L. Hammer, C. Sobel, M. Gubo, K. Heinz, M. A. Schneider, F. Mittendorfer, and J. Redinger, "Self-organized growth, structure, and magnetism of monatomic transition-metal oxide chains," Phys. Rev. Lett. 117(4), 046101 (2016).
- ⁴¹E. E. Fullerton, I. K. Schuller, H. Vanderstraeten, and Y. Bruynseraede, "Structural refinement of superlattices from x-ray diffraction," Phys. Rev. B 45(16), 9292–9310 (1992).
- ⁴²I. K. Schuller, "New class of layered materials," Phys. Rev. Lett. 44(24), 1597–1600 (1980).
- ⁴³T. M. Willey, M. Bagge-Hansen, J. R. I. Lee, R. Call, L. Landt, T. V. Buuren, C. Colesniuc, C. Monton, I. Valmianski, and I. K. Schuller, "Electronic structure differences between H₂-, Fe-, Co-, and Cu-phthalocyanine highly oriented thin films observed using NEXAFS spectroscopy," J. Chem. Phys. 139(3), 034701 (2013).
- ⁴⁴G. Chen, J. Zhu, A. Quesada, J. Li, A. T. N'Diaye, Y. Huo, T. P. Ma, Y. Chen, H. Y. Kwon, C. Won, Z. Q. Qiu, A. K. Schmid, and Y. Z. Wu, "Novel chiral magnetic domain wall structure in Fe/Ni/Cu (001) films," Phys. Rev. Lett. 110(17), 177204 (2013).
- 45X. Chen, Y.-S. Fu, S.-H. Ji, T. Zhang, P. Cheng, X.-C. Ma, X.-L. Zou, W.-H. Duan, J.-F. Jia, and Q.-K. Xue, "Probing superexchange interaction in molecular magnets by spin-flip spectroscopy and microscopy," Phys. Rev. Lett. 101(19), 197208 (2008).
- ⁴⁶Z. G. Yu, "Spin-orbit coupling and its effects in organic solids," Phys. Rev. B 85(11), 115201 (2012).
- ⁴⁷P. S. Miedema, S. Stepanow, P. Gambardella, and F. M. F. de Groot, "2p x-ray absorption of iron-phthalocyanine," J. Phys. 190, 012143 (2009).
- ⁴⁸S. Grytsiuk, J. P. Hanke, M. Hoffmann, J. Bouaziz, O. Gomonay, G. Bihlmayer, S. Lounis, Y. Mokrousov, and S. Blügel, "Topological-chiral magnetic interactions driven by emergent orbital magnetism," Nat. Commun. 11(1), 511 (2020).
- ⁴⁹R. Naaman, Y. Paltiel, and D. H. Waldeck, "Chiral molecules and the electron spin," Nat. Rev. Chem. 3(4), 250–260 (2019).
- 50F. Torres, M. Kiwi, N. M. Vargas, C. Monton, and I. K. Schuller, "Chiral symmetry and scale invariance breaking in spin chains," AIP Adv. 10(2), 025215 (2020)